Impact of Junction Formation Method and Surface Roughness on Single Molecule Conductance

ARTICLE *in* THE JOURNAL OF PHYSICAL CHEMISTRY C · APRIL 2009

Impact Factor: 4.77 · DOI: 10.1021/jp811142d

Impact of Junction Formation Method and Surface Roughness on Single Molecule Conductance

Wolfgang Haiss,* Santiago Martín, Edmund Leary, Harm van Zalinge, Simon J. Higgins, Laurent Bouffier, and Richard J. Nichols

Centre for Nanoscale Science and Department of Chemistry, University of Liverpool, Crown Street, Liverpool L69 7ZD, U.K.

Received: December 17, 2008; Revised Manuscript Received: January 22, 2009

In recent years, several experimental studies have shown that different values of single molecule conductance can be observed for the same type of molecule. Although this observation has been tentatively attributed either to differing molecular conformations or to differing contact geometries, the reason for the different conductance groups remains still unclear. To elucidate this issue, a comparison of four different experimental methods to measure single molecule conductance is presented here for the case of alkanedithiols between gold electrodes, which is considered to be a model system. Three different fundamental conductance groups exhibiting low, medium, and high conductance, respectively, were observed for each molecule. The comparison of measurements performed on surface areas with different step densities reveals that the medium (high) conductance group can be attributed to the adsorption of one (two) contacting S atoms at step sites, whereas the low conductance group can be attributed to molecules adsorbed between flat surface regions. This finding is corroborated by a gap separation analysis for the different conduction groups, by matrix isolation measurements, and by a comparison of the results presented here with conductance measurements performed on self-assembled monolayers. The results presented here help to resolve apparent discrepancies in single molecule conductance measurements and are of general significance for molecular electronics and electrochemistry, since they show how molecular conductance is influenced by the contact morphology and, thus, by the atomic structure of the substrate surface.

1. Introduction

Electron transfer through organic molecules has traditionally attracted considerable interest due to its important role in electronic and biological processes. Early measurements performed in frozen glasses using a laser pump−probe method[1] facilitated the determination of electron transfer rates, as did electrochemical measurements involving laser pulse heating[2] of self-assembled monolayers. Due to the advent of micromechanical processing methods, experiments could be performed which allowed the *direct* measurement of the electronic properties of small groups of self-assembled monolayers in nanopores,[3] mechanically controllable break junctions,[4−6] and conducting probe AFM[7,8] (CP-AFM). The first clear statistical evidence that conductance measurements on *single* molecules can be performed resulted from CP-AFM studies performed by Cui and Lindsay on single alkanedithiol molecules isolated in a monothiol matrix where the top contact to the molecule was realized by gold nanoparticles.[9,10] The latter method will be referred to as the matrix isolation method.

In 2003, Xu and Tao[11] and Haiss et al.[12] demonstrated that the electronic properties of *single* molecules can be studied by a statistical analysis of molecular junctions which were repeatedly formed in an STM, either in organic liquids[11] or under electrochemical conditions.[12] Xu and Tao used an in situ break junction (BJ) method in which mechanical contact of the tip with the metal surface was established in an organic liquid containing α,ω-dithiol molecules before the tip was retracted. The tunneling current versus distance curves obtained during retraction of the tip exhibited characteristic current plateaus at integer multiples of a fundamental current value as revealed by statistical analysis. This behavior was assigned to the presence of an integer number of molecules in the gap. The method of Haiss et al., on the other hand, which will be referred to as the $I(s)$ method (current I and distance s), was performed on substrates with a low coverage phase of flat-lying α,ω-dithiol molecules, and *no* contact between the tip and the sample was established before the tip was retracted, but nevertheless, the $I(s)$ curves exhibited current plateaus at integer multiples of a fundamental current value.[12,13] This behavior has been explained as the result of a spontaneous formation of molecular bridges between tip and sample; these were later found to be also directly observable in the time domain.[14]

Surprisingly, these two seemingly similar STM-based methods applied to the same system resulted in very different conductance values. For example the single molecule conductance values (σ_M) for a 1,8-octanedithiol molecule between gold electrodes determined with the BJ method (∼20 nS) were a factor of ∼20 larger than the values determined with the $I(s)$ method (∼1 nS). In 2004, Haiss et al. showed that both high and low current steps could be observed in the BJ method if sufficient sensitivity was used to observe the smaller steps.[14] It was tentatively suggested that these different conductance values arise from differing contact configurations or ways of forming the junctions.[14] In 2006, Li et al. presented a more detailed analysis[15] showing that the BJ method results in (at least) two different groups of fundamental conductance values, both of which were substantially larger than the results of the $I(s)$ method. More recently, other groups have also confirmed the

* Corresponding author. E-mail: haiss@liv.ac.uk.

10.1021/jp811142d CCC: $40.75
Published on Web 03/17/2009

existence of several groups of conductance values using similar methods. [16−19]

Since both the BJ and $I(s)$ methods have now been adapted in more or less modified forms by a number of groups,[16,18−27] the precise origin of the different conduction values remains a subject of interest, as does the finding that different measurement conditions or techniques can favor different conductance values. This is clearly an important issue to address since these differences give rise to apparent inconsistencies in the literature. In this manuscript, we provide new experimental observations to explain these apparent inconsistencies. This is achieved by comparing experimental results from four different experimental techniques, with an emphasis on the role of the surface morphology.

2. Methods

A "molecular imaging" STM in conjunction with the Picoscan 4.19 Software was used for all measurements. Commercial gold on glass samples with a chromium adhesive layer (Arrandee) were flame-annealed immediately prior to use. Molecules were then adsorbed from toluene solutions, and finally, all samples were thoroughly washed in ethanol and blown dry with nitrogen. Gold STM tips were freshly prepared for each experiment by etching of a 0.25 mm Au wire (99.99%) in a mixture of HCl (50%) and ethanol (50%) at +2.4 V.[28] All the experiments presented here have been performed in air. However, to see if the presence of oxygen or water influences the results, we have repeated some experiments in a hermetically sealed chamber which was purged for one hour prior to the experiments with pure nitrogen, but no systematic differences could be detected between the different environments (air or N_2). A bias voltage of 0.6 V (tip positive) was used throughout (except for the collection of the $I(V)$ data) to facilitate a comparison between the different methods. This bias voltage facilitated measurements of the length dependence of σ_M at constant voltage over an extended conductance range, since the current measured for dodecanedithiol was still significantly above the current amplifier noise, which would not have been the case at much lower voltages. The α,ω-alkanedithiols were used as received from Aldrich (reagent grade), except for 1,12-dodecanedithiol, the synthesis and characterization of which is described in the Supporting Information.

All current and conductance histograms presented in this paper were displayed on a logarithmic current or conductance scale, since the observed σ_M values are distributed over a wide range, whereas the relative width of the conductance peaks was found to be approximately constant, and hence, on a linear conductance scale, not all conductance peaks can be resolved using the same bin size. The error bars for the average conductance and current data presented in this paper represent the standard deviation of the conductance values or current values collected for a particular conductance group.

For the $I(s)$ measurements,[12,14] following temporary disablement of the feedback loop, the tip was retracted from the position defined by the set-point values of tunneling current (I_0) and tunneling voltage (U_0) to a distance of +2 nm with a rate of 40 nm s^{-1}. Break junction experiments were realized by performing $I(s)$ scans from −1 to +2 nm at a scan rate of 3 nm s^{-1}. To determine the absolute tip−sample separation (s) at which a molecular wires breaks in the $I(s)$ scans, the set-point parameters (I_0, U_0) have to be converted to an absolute gap separation (s_0). This was done in the following way: The exponential dependence of I on s (in the absence of a molecular wire in the gap) is determined from $I(s)$ scans recorded in the absence of molecular wires between tip and sample. Such $I(s)$ scans have been performed at regular intervals during the measurement. Averaging the slope of the corresponding d ln(I)/ds curves, (d ln(I)/ds was typically on the order of (10 ± 1.5) nm^{-1}) provides the conversion factor between ΔI and Δs. Assuming that the conductance at the point where the tip would make mechanical contact with the surface is the conductance quantum G_0 ($G_0 = 2e^2/h$) provides the basis for an absolute calibration of the gap separation at a given current according to eq 1:

$$s(I) = \frac{\ln(G_0 \times U_0/I)}{\mathrm{d}\ln(I)/\mathrm{d}s} \quad (1)$$

Conductance values of G_0 have, indeed, been observed experimentally at the mechanical contact point,[6] and hence, eq 1 should provide a reasonable calibration of the absolute distance between tip and sample.

For matrix isolation (MI) experiments, two different sample preparation methods have been used: A self-assembled monolayer (SAM) of mixed alkanethiols and alkanedithiols was prepared by immersing the samples in a mixture of 10^{-3} M alkanethiol and 10^{-6} M alkanedithiol for 5 min. The samples were then thoroughly washed in ethanol, blown dry with nitrogen, and immediately immersed for ∼5 min in a ∼1 nM solution of gold nanoparticles (d = (5 ± 1) nm) in toluene. Finally, the samples were washed in ethanol and blown dry in N_2. This preparation method will be referred to as the "MI-mix method". It should be noted here that a short immersion time in the mixed solution is necessary to avoid segregation of the dithiols and, hence, island formation which was observed for long immersion times. The other preparation method, which will be referred to as the "MI-replacement method" was realized in the following way: Samples were first immersed in a 20 mM solution of alkanethiols for 24 h. After ethanol wash and drying in N_2, these samples were immersed in 2 mM alkanedithiol solution for 5 min; again washed and dried; and finally, immersed for ∼10 min in a ∼1 nM solution of gold nanoparticles (d = (5 ± 1) nm) in toluene. The synthesis of the gold nanoparticles (GNPs) is described in reference 29.

3. Results and Discussion

3.1. The Conductance of Octanedithiol Measured by Four Different Methods. ***3.1.1. The I(s) Method.*** Figure 1a and 1b show typical $I(s)$ example curves observed in the presence of octanedithiol (ODT). These $I(s)$ curves exhibit typical current jumps (indicated by the arrows) that are attributed to the breaking of a molecular wire that was attached between tip and sample at the start of the scan. Two different fundamental types of current jumps can be observed in these $I(s)$ curves. One group occurs at conductance values of ∼1 nS (Figure 1a), and another group, at conductance values of ∼3.7 nS (Figure 1b). These two groups dominate the logarithmic conductance histogram in Figure 1c, which was constructed from 518 $I(s)$ curves taken at different random locations of the sample. The fundamental peak at ∼1 nS will be referred to as A_1, whereas the peak at 3.7 nS will be referred to as B_1. In addition to these peaks, there are two smaller peaks visible at approximately twice the fundamental current values (A_2 at 1.8 nS and B_2 at 7.2 nS). According to earlier work,[12,14] the peaks with subscript 1 are attributed to a single molecule bridging the gap, whereas the peaks with subscript 2 are attributed to two molecules. The single-molecule conductance values (σ_M) of the two fundamental

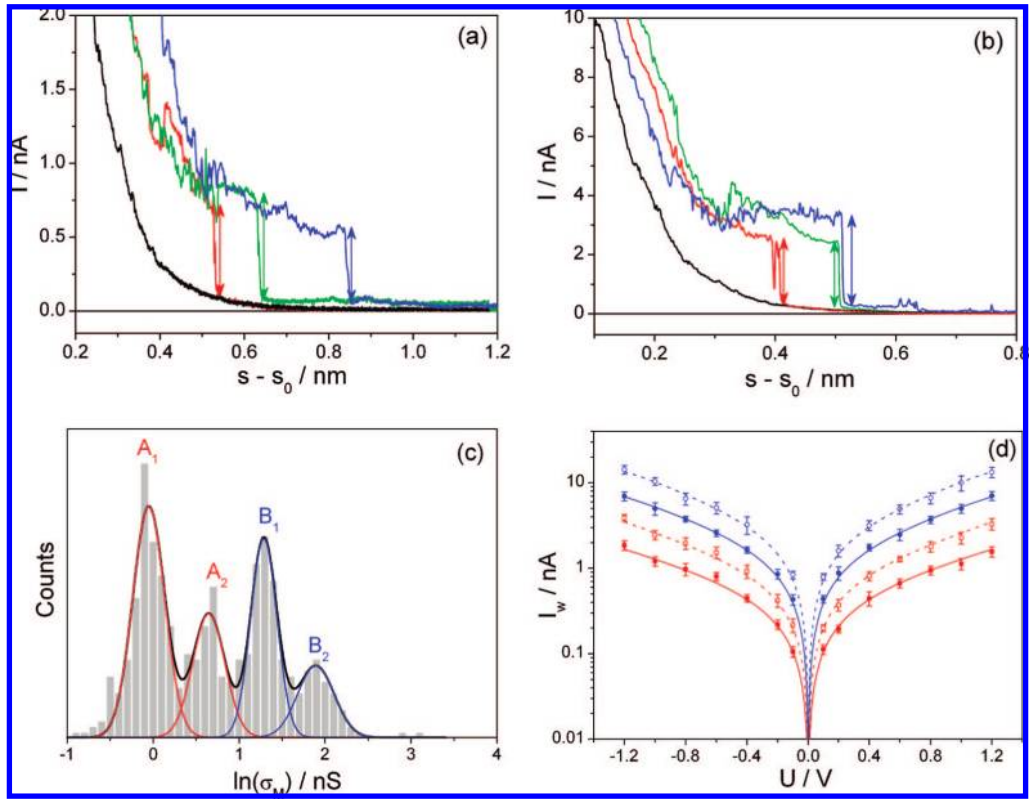

Figure 1. $I(s)$ curves obtained on Au(111) in the presence of ODT at $U_0 = 0.6$ V and $I_0 = 20$ nA (a and b). Predominantly, two fundamental groups of current jumps were observed: group A_1 current jumps, shown in panel a, corresponding to a conductance value of ~1 nS, and group B_1 jumps, shown in panel b, corresponding to a conductance value of ~3.7 nS. The black curves in panels a and b show an exponential decay curve in the absence of molecular wire formation for comparison. In the logarithmic conductance histogram of 518 current jumps shown in panel c groups A_1 and B_1 are marked together with conductance peaks at approximately twice (A_2, B_2) the fundamental conductance values together with Gaussian fit curves. Panel d shows the voltage dependence of the plateau current for the four different conductance groups (A_1, red filled circles; A_2, red open circles; B_1, blue filled circles and B_2, blue open circles), measured at a constant gap resistance of 30 MΩ together with a Simmons fits. All results were collected on a sample immersed for ~20 s in a 2×10^{-2} M solution of ODT in toluene.

conductance groups in the conductance histogram of Figure 1c are in perfect agreement with recently published results of Li et al.[16]

Figure 1d shows the voltage dependence of the jump current for the different conductance groups. These $I(U)$ measurements were performed at a constant gap resistance of 30 MΩ to hold the tip sample separation approximately constant during these experiments. The height of the current jumps (I_w) increases clearly with the applied voltage (U), and the $I_w(U)$ relation can be fitted well with the modified Simmons equation[3] (lines in Figure 1d).

$$J = \frac{e}{4\pi^2\hbar d^2}\left\{\left(\Phi_B - \frac{eV}{2}\right)\exp\left[-\frac{2(2m)^{1/2}}{\hbar}\alpha\left(\Phi_B - \frac{eV}{2}\right)^{1/2}d\right] - \left(\Phi_B + \frac{eV}{2}\right)\exp\left[-\frac{2(2m)^{1/2}}{\hbar}\alpha\left(\Phi_B + \frac{eV}{2}\right)^{1/2}d\right]\right\} \quad (2)$$

J denotes the charge density, which was calculated from the observed current values by assuming that the surface area occupied by a single ODT molecule is 0.217 nm^2, which is the area occupied by a single molecule in a $(\sqrt{3} \times \sqrt{3})$R30° structure on Au(111). m and e represent the mass and the charge of an electron, respectively; and d denotes the width of the tunneling barrier, which was assumed to be the through-bond distance between the sulfur atoms in ODT (1.44 nm) calculated with a molecular modeling program. Φ_B and α are the fit parameters, where Φ_B is the effective barrier height of the tunneling junction, and α is related to the effective mass of the tunneling electron. The exponential decay factor (β_0) can be calculated from the effective barrier height (Φ_B) and the fit parameter α according to eq 3:[3]

$$\beta_0 = \frac{2(2m)^{1/2}}{\hbar}\alpha(\Phi_B)^{1/2} \quad (3)$$

TABLE 1: Parameters Resulting from a Fit of the Experimentally Observed I(V) Characteristic to Equation 2

method	Φ_B/eV	α	β_0 per CH_2	J at 1 V/10^5 A cm^{-2}	ref
$I(s)$ A_1	1.45 ± 0.1	0.42 ± 0.04	0.79	5.8	this work
$I(s)$ A_2	1.26 ± 0.2	0.45 ± 0.03	0.79	6.0	this work
$I(s)$ B_1	0.80 ± 0.04	0.43 ± 0.02	0.60	24.0	this work
$I(s)$ B_2	0.75 ± 0.07	0.46 ± 0.03	0.62	23.5	this work
nanopore	1.20	0.59	1.01	0.93	3
TVS	1.28 ± 0.12				30
theory		0.54			31

The exponential decay factor at zero bias (β_0) results from the effective barrier height (Φ_B) and the fit parameter, α, according to eq 3. Also listed are the current densities at 1 V.

In Table 1, the parameters resulting from the fit of the experimentally observed $I(U)$ characteristic to the modified Simmons equation (eq 2) are shown. Also shown in Table 1 is the exponential decay factor (β_0) resulting from the effective barrier height (Φ_B) and the fit parameter, α, according to eq 3. The theoretically calculated value for the effective mass of the

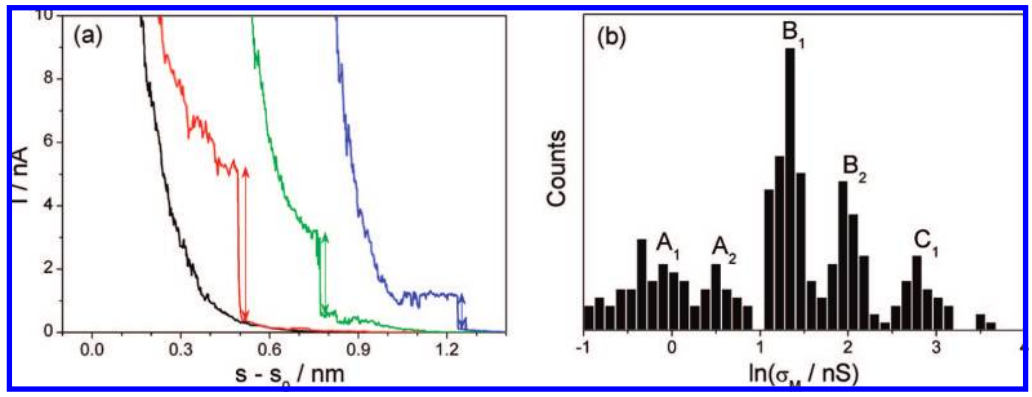

Figure 2. STM break junction results for octanedithiol between gold contacts. (a) Example scans; the current jump height determined for each curve is indicated with an arrow; the black curve shows an exponential decay curve in the absence of a molecular wire formation for comparison. The green and blue curves have been shifted by 0.3 and 0.6 nm, respectively, for clarity. (b) Logarithmic conductance histogram of 279 current jumps. All results were collected on a sample immersed for ~20 s in a 2×10^{-2} M solution of ODT in toluene.

tunneling electron in a CH_2 chain, m^*, as calculated by Tomfohr and Sankey was translated to an α value ($\alpha^2 = m^*$) to facilitate a comparison with the experimentally measured values.

The value of Φ_B for conductance group A (1.3 ± 0.15 eV) determined from the $I(s)$ experiments is in good agreement with the Φ_B value resulting from nanopore experiments (1.2 eV) and from transition voltage spectroscopy experiments (1.28 eV).[30] In addition, the exponential decay constant (β_0) calculated from eq 3 for the conductance group A is in reasonable agreement with the direct determined value (0.89 per CH_2, see section 3.4) and in good agreement with the results of measurements performed on SAMs (0.84 per CH_2[3,32]). The absolute current density (at 1 V) of conductance group A measured with the $I(s)$ technique is larger than the current density observed in the nanopore experiments by approximately a factor of 6. This may be attributed to the possibility that not all molecules of the self-assembled monolayer (SAM) are connected to the electrode in the nanopore experiments. Assuming that only 1 in 6 molecules is connected yields quantitative agreement with the experiment, and this assumption does not seem unrealistic, given some degree of interface roughness which may result when evaporating the gold top-contact onto a SAM of ODT on Au(111). A comparison of the fit parameters in Table 1 helps to identify the conductance group A with a "normal" adsorption geometry, which is encountered in experiments on SAMs since the fit parameters of conduction group B are significantly different from those encountered in SAM experiments.

3.1.2. The BJ Method. We now turn to the break-junction method.[11,15] In this method, mechanical contact between the tip and the surface is established. The gold tip is then withdrawn to the point where the Au−Au contact between tip and substrate is broken. Molecular junctions are then formed in the gap, and the cleavage of these junctions is monitored as the tip is withdrawn from the surface, resulting in characteristic current steps (Figure 2a), which are then statistically represented in current or conductance histograms. Figure 2b shows a conductance histogram for ODT. Similar to the $I(s)$ results, multiple conductance peaks are seen, and these are labeled using the same notation as Figure 1. At conductance values of ~17 nS, there is an additional, smaller peak visible (C_1).

3.1.3. The I(t) Method. A further method for measuring single molecule conductance (σ_M) is the $I(t)$ technique.[14] This technique involves holding the Au STM tip at a given distance above the substrate while monitoring current jumps as molecular wires stochastically form a bridge between the tip and the substrate and subsequently break. The results of this method are detailed in the Supporting Information section entitled "Single Molecule Conductance Measurements Using the $I(t)$ Method". In brief, it was found that the σ_M values and their voltage dependence measured with the $I(t)$ technique at low set-point currents (i.e., at tip sample separations comparable to the length of the molecule) are consistent with the A_1 group results of the $I(s)$ technique. At higher set-point currents (i.e., at tip sample separations much smaller than the molecular length), the conductance increases substantially. It also was found that the height of the current jumps at fixed set-point parameters increases with surface roughness.

3.1.4. Matrix Isolation Method. The fourth technique we have used is that developed by Cui and Lindsay,[9,10] which we refer to here as the "matrix isolation" (MI) method. As described in the Methods section, octanedithiol is highly diluted in a self-assembling monolayer of octanethiol, and this surface is exposed to a solution of gold nanoparticles. As gold nanoparticles preferentially attach to the thiol terminus of the dithiol, a nanoscale junction is formed with one or more dithiol molecules linking the nanoparticle and surface. These structures then provide the test bed for electrical characterization using either a current-sensing AFM tip[10] or, in our case, an STM tip (schematically illustrated in Figure 3a). Figure 3b shows a STM image of two Au nanoparticles (height ~ 5 nm) on a Au(111) surface covered with a mixture of octanethiol (OT) and ODT (1000:1). A GNP size of 5 nm has been chosen, since it has been demonstrated that Coulomb blockade effects are negligible in this size range, and hence, the molecular resistance can be determined directly from the measured current to good approximation.[10]

To measure the current through the ODT molecules attached between the GNP and the Au(111) surface, the tip was placed on top of the particle under investigation, and the tip was then moved toward the particle from a distance s_0, which resulted in typical current jumps as shown in Figure 4a−c. Three fundamental types of current jumps were observed in these experiments: small current jumps referred to as group A (Figure 4a), medium size current jumps (group B; Figure 4b) and large jumps (group C; Figure 4c), with the same label (A, B or C) being given as before, since they correlate well with those described in the previous text.

The conductance histogram in Figure 5a constructed from 348 current jumps observed on samples produced with the MI-mix method exhibits peaks at the fundamental current values of group A at (1.00 ± 0.17) nS, group B at (3.9 ± 0.7) nS, and group C at (18.6 ± 2.0) nS. It should be emphasized that in

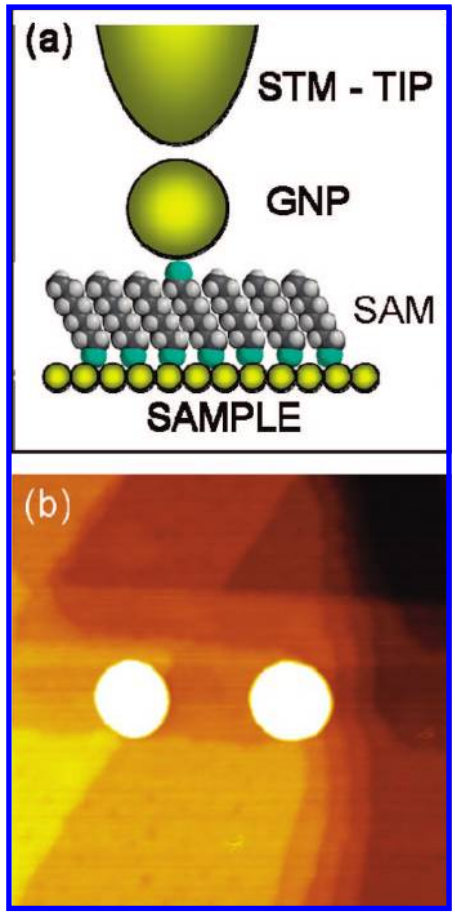

Figure 3. (a) Schematic representation of the matrix isolation method. To measure the conductance of a dithiol molecule embedded in a monothiol SAM, the STM tip approaches the gold nanoparticle. (b) STM image of two GNPs on Au(111) covered with a OT/ODT SAM; image size 80 nm × 80 nm.

constructing such a histogram, many different nanoparticles were measured for the statistical representation. From these observations, it can be concluded that also in a densely packed SAM, the ODT molecules give rise to three main groups of conductance peaks. In addition, peaks at approximately twice the fundamental current values (A_2 at (1.88 ± 0.24) nS and B_2 at (7.8 ± 0.9) nS) are also visible. Figure 5b shows a conductance histogram obtained after using the replacement method to prepare the samples for the matrix isolation experiments. As for the MI-mix methods, group A, B and C events are observed, although the group B events dominate the conduction histogram when the replacement method is used, whereas group A events dominate the conduction histogram when the MI-mix method is used. Reasons for these differences between the MI-mix and MI-replacement methods are discussed later in the text.

3.1.5. Comparison of the Conductance Values Obtained for ODT. The σ_M values of ODT observed for the various types of experiments as discussed above are compared on a logarithmic scale in Figure 6a, where the average conductance value for the different conduction groups are represented by horizontal lines (A_1, 0.96; A_2, 1.87; B_1, 3.82; B_2, 7.9; C_1, 17.0; C_2, 34.7 nS). These average conductance values are contained in the error bars for all of the data points, indicating good agreement between the different experimental methods. In Figure 6b, the ratio of the number of group B (N_B) to the number of group A events (N_A) is plotted for each of the various experiments. Using the BJ method, group B clearly dominates the conductance spectrum. For the MI-replacement method experiment (MI-R

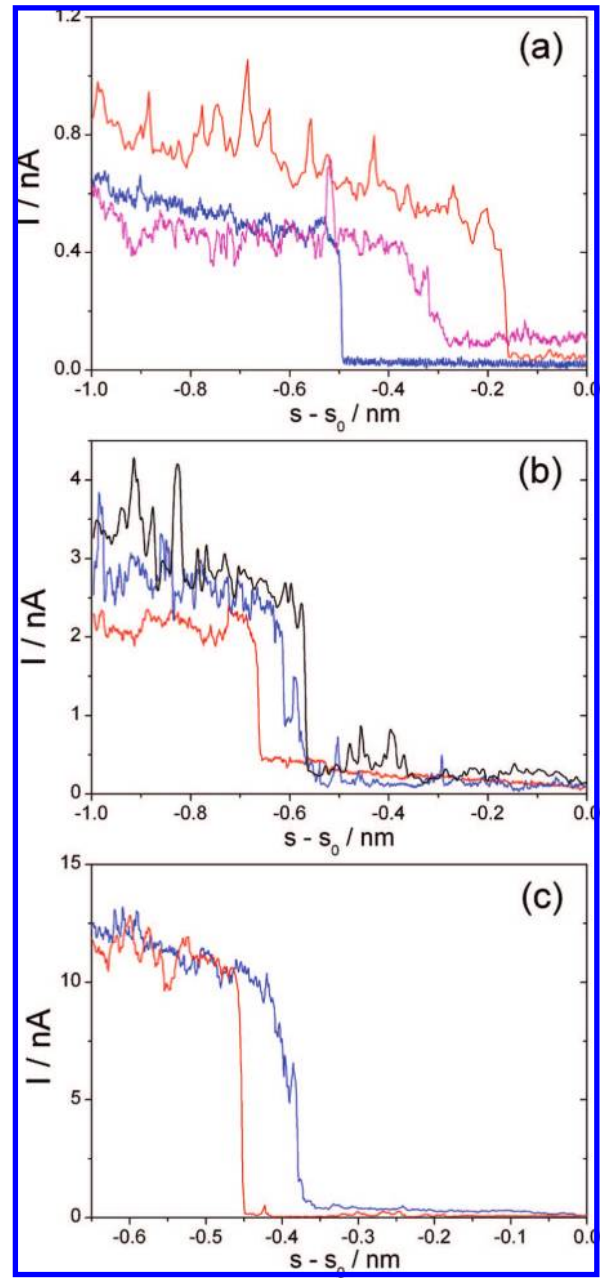

Figure 4. Current−distance approach curves obtained by the MI-mix method for ODT between gold contacts; U_0 = 0.6 V; I_0 = 0.1 nA. Three different types of $I(s)$ curves were observed corresponding to conductance values of ∼1 nS (a), ∼4 nS (b), and ∼18 nS (c).

in Figure 6), the N_B/N_A ratio is substantially larger than for the MI-mix method experiments. It is clear from Figure 6b that the differing techniques favor different conductance groups. For instance, using the $I(t)$ technique at low set-point current values, only group A events are observed. On the other hand, in the BJ techniques and matrix replacement methods, group B events give the predominant conductance peaks. In the following section, we explore this issue further by controlling the morphology of one of the metal contacts.

3.2. Controlling the Contact Morphology. An idealized single molecule electrical measurement would allow precise determination of the junction morphology during the determination of the electrical response. Such experiments have not been realized, and the difficulty in achieving this in a STM experiment is compounded by the general uncertainty in the exact atomic configuration of the tip apex. It is generally

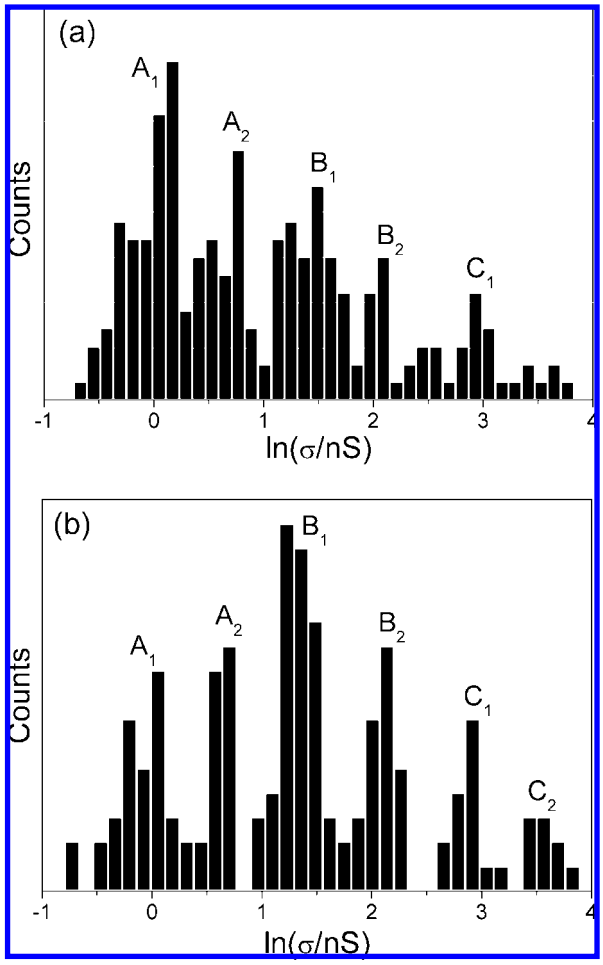

Figure 5. Conductance histograms resulting from MI experiments using two different preparation methods, the "mix method" (a) or the "replacement method" (b) for matrices of ODT in OT on Au(111). This conductance data was obtained by recording 347 (a) and 160 (b) current−distance approach curves with the STM tip positioned above a wide selection of individual GNPs.

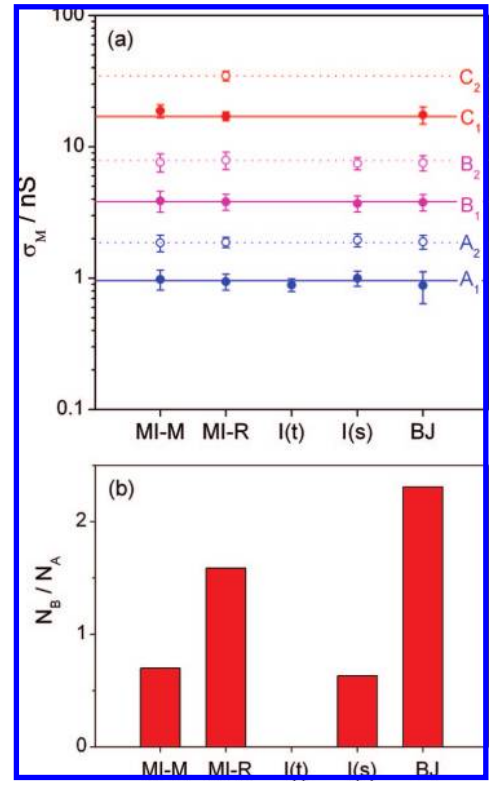

Figure 6. (a) Comparison of the σ_M results for ODT obtained by different methods marked on the *x*-axis (methods: MI-M = matrix isolation mix, MI-R = matrix isolation replacement, $I(t)$, $I(s)$, and BJ = break junction). The average conductance values of the three fundamental conductance groups are indicated by horizontal lines. (b) Ratio of the number of group B events to the number of group A events (N_B/N_A) obtained with the different techniques.

accepted, indeed necessitated, that for high resolution STM imaging, the tip is not flat, but rather, structured on the atomic scale. For this reason, we cannot control the morphology of the STM tip in our experiments, but we can control the substrate morphology from atomically flat regions to highly structured rough surface areas. Through measurements on differing surface morphologies, we will demonstrate in the following text that different morphologies of one of the contacts (the substrate) has an effect on the distribution of σ_M values. We will use this information to make inferences about the origin of the distribution of σ_M values seen in Figures 1 and 6.

In Figure 7, the results of $I(s)$ measurements that were performed on a flat Au(111) terraced region on the sample for a 2×10^{-4} M solution of ODT immersed in toluene for 20 s are shown. Figure 7b shows an STM image of the surface, together with a conductance histogram (Figure 7a) taken on the atomically flat region of the sample; the central flat terrace has a width of about 40 nm. There are two conductance peaks visible, corresponding to a conductance value of 0.9 nS (A_1) and 1.88 nS (A_2). B and C peaks do not feature in this histogram. When comparing Figure 7 to Figure 1c, which features data accumulated on a wide range of differing surface regions, it can be concluded that the A group of peaks can be selectively favored if measurements are carried out on atomically smooth terraces.

We now explore the effect of increasing the surface roughness. In Figure 8a, the conductance histogram has been taken on a slightly stepped region (see the STM image that is presented in Figure 8b) that exhibits, in addition to the A_1 and A_2 peaks, B_1 and a B_2 peaks. The B peaks dominate in the rough area of the sample (Figure 8c and STM image in Figure 8d). Also in the BJ measurements (Figure 8e), the B group dominates and an additional peak at ~17 nS (C_1) is observed. Figures 7 and 8 demonstrate clearly that the ratio of group B to group A events increases with increasing step density or surface roughness, and hence, it seems reasonable to attribute the B group to an adsorption geometry where the molecular wire is adsorbed at a step edge of the sample (or similar high coordination defect site). This view is consistent with the finding that the conductance group B dominated the conductance histogram of $I(t)$ experiments on rough surfaces, whereas group A dominated the $I(t)$ conductance histogram on atomically flat surfaces (these data are shown in the Supporting Information).

3.3. Analysis of the break off length for the different conductance groups. Three possible adsorption geometries together with their corresponding maximum tip−sample separation are schematically illustrated in Figure 9. At relatively large tip−sample separations (s_A in Figure 9a), it is geometrically impossible for the ODT molecule to adsorb on the lower terrace of a step edge, whereas at somewhat closer tip−sample separation (s_B in Figure 9b) step edge adsorption is possible whenever such a site is available, otherwise the molecule may undergo tilting. At even closer tip−sample separation (s_C in Figure 9c) step edge adsorption is possible at both sides of the molecule.

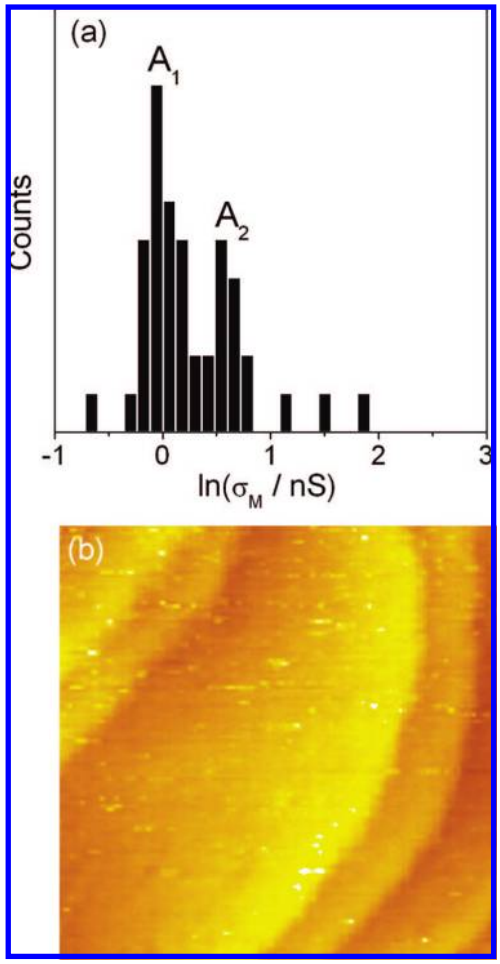

Figure 7. (a) Conductance histogram of ODT on Au(111) obtained using the $I(s)$ method; $U_0 = 0.6$ V; $I_0 = 6$ nA. (b) STM image of the area where the $I(s)$ measurements were performed; image size 80 nm × 80 nm.

The average of the absolute tip sample separations (s_{break}) where molecular wires of a given conductance group were found to break in the $I(s)$ scans for the different conductance groups was determined from the position of the observed current jumps using Equation 1 for calibration. The experimentally determined s_{break} value for A_1 events (1.32 ± 0.13 nm), is very close to the calculated value of s_A (1.38 nm, see Figure 9a). The same holds for group B (1.15 nm calculated; (1.24 ± 0.16) nm measured) and for group C (0.93 nm calculated; (1.00 ± 0.21) nm measured), and hence, the assignment of group B_1 to a geometry depicted in Figure 9b and the assignment of group C_1 to a geometry depicted in Figure 9c is supported by this observation. Here, it is important to mention that if $I(s)$ or $I(t)$ measurements are performed at small set-point currents (i.e. at relatively large tip−sample separations) groups B and C are generally not observed. This is consistent with earlier studies[14] and further supports the model depiction in Figure 9, since at large s values, only group A events can occur, more or less independent of the sample and tip morphology.

Attributing conductance group B to adsorption at step edges is also corroborated by an analysis of $I(s)$ scans, in which both a group A and a group B plateau can be found. Figure 10a shows an example of such scans which have been frequently observed during the measurements. A histogram of the relative distance (s_{rel}) between the end of the B plateau and the end of the A plateau is presented in Figure 10b. The average distance between the A and B plateaus (0.21 ± 0.10 nm) is close to the height of a monatomic step on Au(111) (0.235 nm), and hence, a sulfur headgroup which is initially adsorbed at the lower atomic terrace of a step edge (conductance group B_1, see Figure 9b) could be pulled up the edge or the defect during retraction of the tip, which may explain the occurrence of two plateaus in one scan. The same explanation may also explain the transitions from group C_1 to group B_1 (see Figure 10b), where the histogram of the average distance between the C and the B plateaus (0.20 ± 0.08 nm) is also close to the height of a monatomic step (see Figure 10d). Interestingly, we have observed $I(s)$ scans similar to the one in Figure 10 also for conformationally rigid molecules and for other head groups where s_{rel} was on the order of the height of a monatomic step throughout.

There is also evidence from the matrix isolation method for assignment of group B (and group C) conductance values, as being related to adsorption sites at step edges. This evidence is supported by the following observation: when the underlying step structure of the Au(111) substrate can be resolved in the STM image, as is the case in Figure 3b, then group B and group C conductance values have been observed if the position of the GNPs and, hence, the adsorption site of the ODT molecule was in close proximity to a step edge. This was the case for both GNPs in Figure 3b, where only group B and group C jumps were observed in repeated measurements performed on these GNPs.

As additional evidence, group B and group C events became more pronounced when the replacement method was used to prepare the samples for the matrix isolation experiments. Figure 5b shows a conductance histogram taken on such a sample, where $I(s)$ scans from a large number of different GNPs are analyzed. The positions of the conductance peaks in Figure 5b (matrix replacement method) are identical within experimental error to those of Figure 5a (matrix mix method), but the ratio of group B to group A is significantly larger in Figure 5b. This observation further corroborates the conclusion that group B events are related to adsorption sites at step edges, since it seems likely that ODT molecules replace OT molecules predominantly at step edges, since there the OT-SAM is not as well-ordered as on atomically flat terraces. Consequently, GNPs on samples produced with the replacement method can be found predominantly at step edges, as has been revealed already by similar experiments performed by Morita et al.,[10] where group B and group C events dominate the conduction histogram.

For completeness, it should be mentioned that the present paper focuses on experimental scenarios in which the alkanedithiols are studied at tip sample separations comparable to the length of the all-trans conformer (i.e., break junction, $I(s)$, matrix isolation, and $I(t)$ studies at small I_0 values). Under these conditions, short, highly folded (gauche rich) conformers cannot contribute to the conduction process, and the temperature dependence of σ_M is thus expected to be negligible here. This was, indeed, shown to be the case for the $I(t)$ method at large tip sample separations[33] and for the break junction method,[15] in which molecules are stretched out prior to breaking. Consistent with that view, temperature-independent tunneling was also observed in experiments performed on self-assembled monolayers of octanedithiol.[3]

3.4. Length Dependence and Comparison with the Results of Other Research Groups. We have applied the various experimental techniques described above to several other alkanedithiols. In the length range from $N = 8$ to $N = 12$, where N is the number of CH_2 groups in the molecule, we have determined the exponential decay factor (β_N) for the three different fundamental conductance groups from the

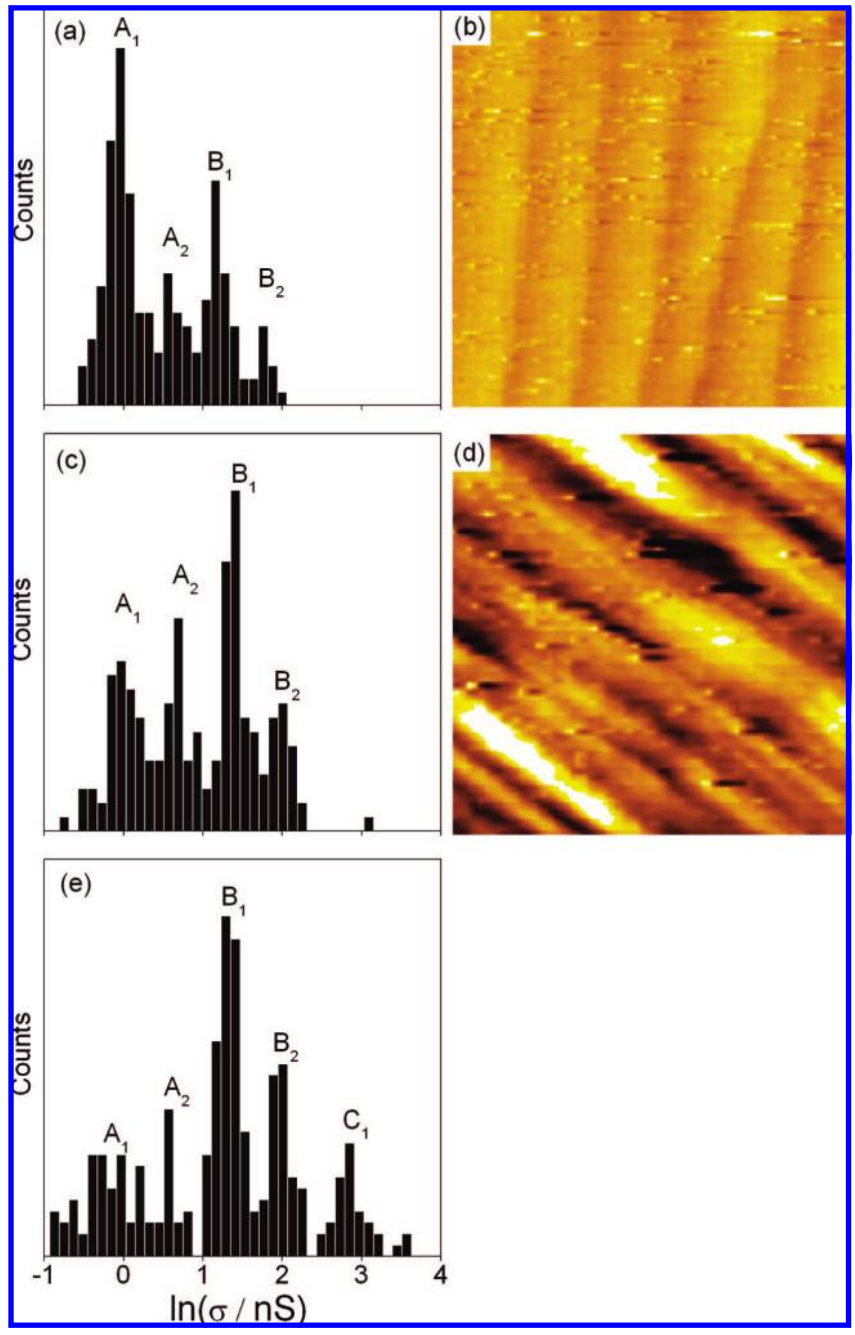

Figure 8. Conductance histograms of ODT on Au(111) taken on surface areas exhibiting different step densities. The ratio of high conductance events (group B) to low conductance events (group A) increases with the step density and/or roughness of the sample. Stepped surface (a);. Rough surface (c); $I(s)$ technique at $U_0 = 0.6$ V; $I_0 = 20$ nA in (a) and (c). The STM images in (b) and (d) (80 nm × 80 nm) have been taken at the location where the histograms of (a) and (c) were obtained and their z-contrast range is 2 nm for both to facilitate comparison. In figure (e) the results of the BJ technique are shown. All results were collected on a sample which was immersed for ~ 20 s in a 2×10^{-2} M solution of ODT in toluene, subsequently washed in ethanol and blown dry with nitrogen.

slope of the linear fits to the experimental σ_M data shown in Figure 11a to be (0.89 ± 0.03) per CH_2 for the A_1 group, (0.89 ± 0.03) per CH_2 for the B_1 group, and (0.93 ± 0.05) per CH_2 for C_1 group. These values are in good agreement with other experiments performed on single alkanedithiol molecules[15,22,23,27] or on small groups of alkanedithiol molecules.[3,7] The observation that the β_N values that we have determined for the different conduction groups are the same (within the error bars) is consistent with the idea that the contact resistance of one sulfur atom (B_1 group) or two sulfur atoms (C_1 group) decreases due to the adsorption at step sites. The contact resistances determined from the intercept of the linear fits in Figure 11a (i.e., the inverse of the conductance for $N = 0$) are (859 ± 23) kΩ for group A_1, (208 ± 6) kΩ for group B_1, and (35.4 ± 1.6) kΩ for group C_1.

The average break-off length determined by the $I(s)$ technique (i.e., the average tip−sample separation at which the molecular wire is broken and, hence, the current jump is observed) is shown in Figure 11b for the A_1 group (squares), where eq 1 was used for calibration. Also shown in Figure 11b are the results of a molecular modeling calculation (circles) assuming adsorption geometries as depicted in Figure 9a for the case of ODT. The agreement between the model calculations and the

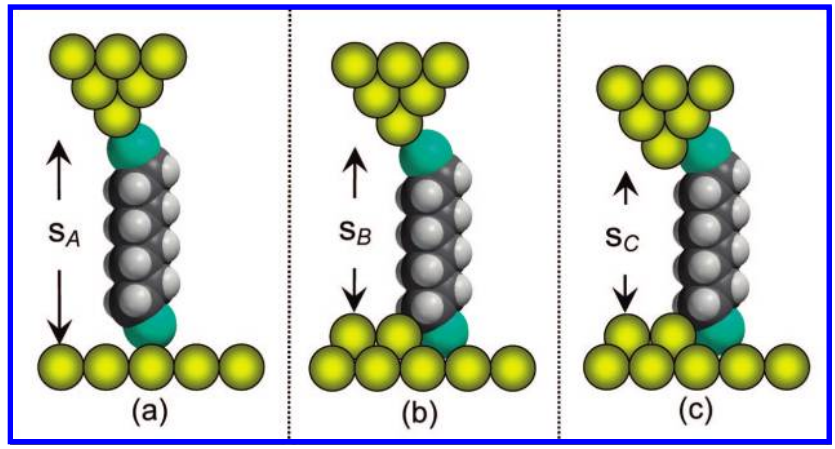

Figure 9. Three possible morphologies of an ODT molecule between gold contacts, roughly to scale. For tip sample separations larger than s_A the molecule cannot bridge the gap between tip and sample (a). Adsorption at step edges may increases the electronic coupling of the molecule to the surface (b). Attachment of both sulfur head-groups to a step edge or to a similar site may result in a further increase of conductance (c). The various tip−sample distances s_A, s_B, s_C are in good agreement with the distances which were experimentally determined for group A, group B and group C events.

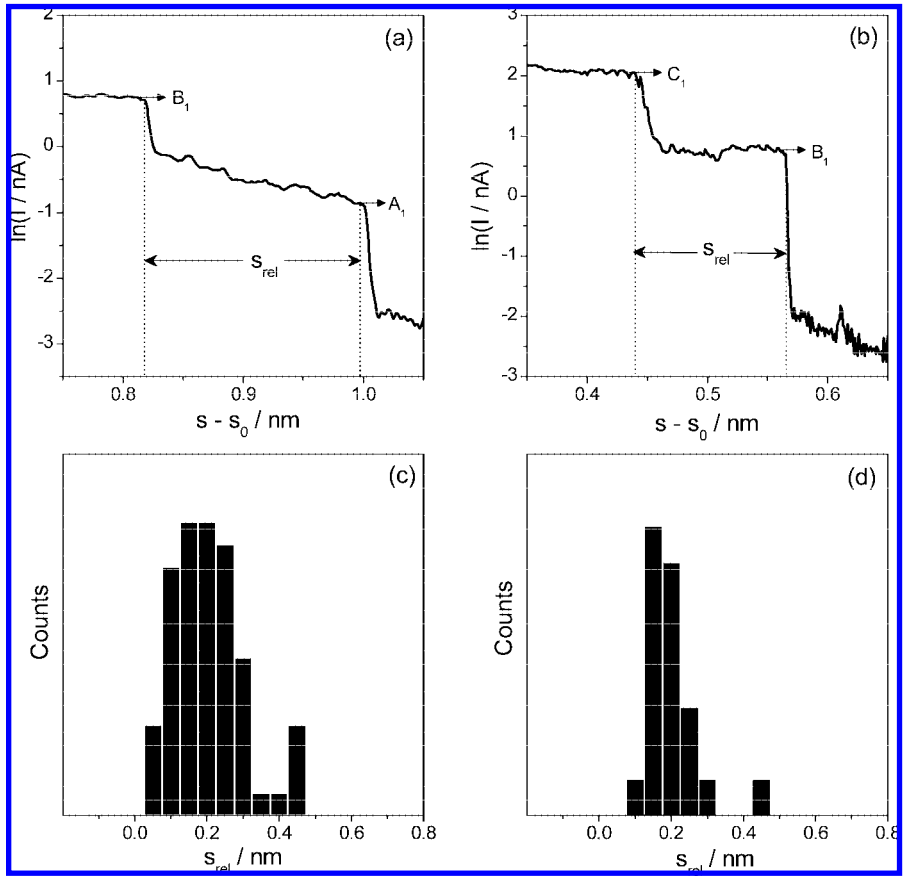

Figure 10. $I(s)$ scan exhibiting both a group B_1 and a group A_1 plateau (a) recorded for ODT on gold. The histogram of the relative distance between the plateau ends (s_{rel} as outlined in panel a) peaks approximately at the height of a monatomic step (c). $I(s)$ scan exhibiting both a group C_1 and a group B_1 plateau (b) recorded for ODT on gold. The histogram of the relative distance between the plateau ends (s_{rel} as outlined in panel b) peaks approximately at the height of a monatomic step (d).These results were collected on a sample that was immersed for ~20 s in a 2×10^{-2} M solution of ODT in toluene, subsequently washed in ethanol, and blown dry with nitrogen.

experimentally measured values over the whole length range indicates that Figure 9a depicts a realistic model for the A_1 group.

Attribution of the A_1 group to an adsorption geometry as depicted in Figure 9a is also supported by theoretical ab initio studies of the Au−ODT−Au system[34] for which a conductance of ~1 nS was calculated, in agreement with the experimental observations. However, somewhat larger conductance values for the Au−ODT−Au system have been reported in other theoretical studies.[21,35,36]

Finally, the conductance values reported here for ODT are compared to the results of other research groups. Li and Tao reported two groups of fundamental conductance values for ODT in their in situ BJ experiments (4 and 19.4 nS)[15] which are consistent with the B_1 and C_1 values reported here, and hence, in the BJ technique, the sulfur atoms may predominantly

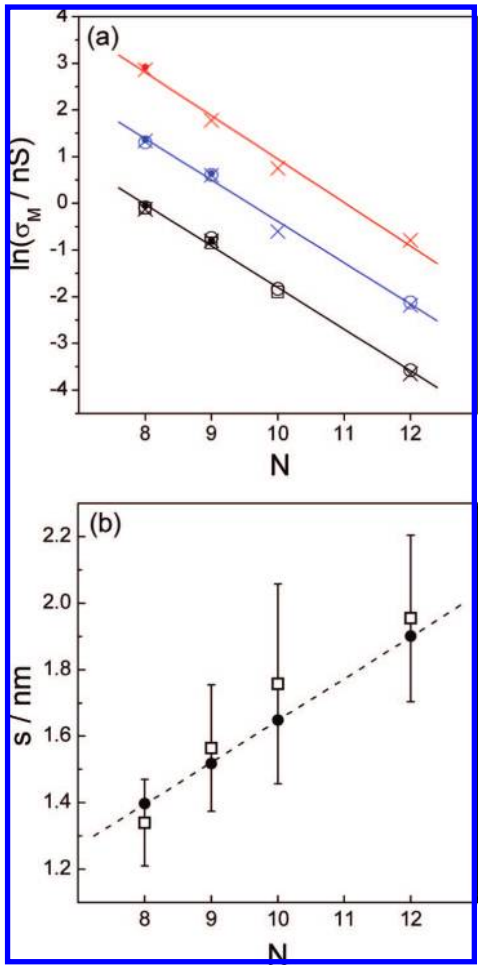

Figure 11. (a) Logarithm of the three single molecule conductance groups (A_1, black; B_1, blue; C_1, red) measured for alkanedithiols between gold contacts as a function of the number of CH_2 groups (N). $I(s)$ technique, open circles; $I(t)$ technique, squares; MI-mix method, small filled circles; BJ technique, crosses. The lines are linear fits to all data, resulting in a slope of (0.89 ± 0.03) per CH_2 for group A_1, (0.89 ± 0.03) per CH_2 for group B_1, and (0.93 ± 0.05) per CH_2 for group C_1. (b) Experimentally determined average break-off length of alkanedithiols (A_1 group) as a function of the number of CH_2 groups measured with the $I(s)$ technique, squares; error bars, ± standard deviation. The results of a molecular modeling calculation are shown as circles, together with a linear fit.

adsorb at a step edge or close to gold ad-atoms, which are inevitably pulled out of the surface during the formation of an atomic gold wire. This explains the lack of the A_1 group in these experiments among other possible reasons rooted in the experimental details (i.e., current range of the amplifier, high retraction speed, high surface coverage). For example, using an amplifier with 1 μA maximum range, it was not possible for us to resolve group A events in the background current noise, especially for fast retraction speeds. However, Li et al.[16] reported recently three fundamental conductance values for ODT ((0.89 ± 0.08), (4.4 ± 0.4), and (21 ± 2) nS) using a modified $I(s)$ technique in which the tip was brought in very close proximity to the surface before retraction, and two current amplifiers were used simultaneously to cover the whole relevant current range. In addition, these values compare well with our results of Table 1. Morita and Lindsay[10] have performed CP-AFM measurements using the MI-replacement method in which two fundamental conductance groups for ODT were found ((5.6 ± 2.3) and (16.1 ± 1.0) nS), which are consistent with our MI results for the B_1 group ((3.9 ± 0.7) nS) and the C_1 group ((18.6 ± 2.0) nS) within the standard deviation. The absence of the A_1 conduction group in these experiments of Morita and Lindsay may be explained by the fact that a substantial load (7 nN) was applied to the AFM cantilever to establish electrical contact between the current-sensing AFM probe and the GNP for the measurement of the conductance. Using the Hertzian model as presented in the supporting material of ref 10, we have calculated the compression of the SAM at 7 nN to be 0.45 nm. This reduced contact gap separation leads to the A conduction group's not being observed under these conditions, which is consistent with the $I(t)$ results presented in the supporting material.

The assertion that the molecular conductance increases when one of the S atoms is attached to a step edge or other high coordination site is consistent with the notion that a higher coordination of the headgroup leads to an increased transmission. This has been qualitatively confirmed by calculations for ODT between planar gold contacts, where it was found that the highly coordinated hollow adsorption site exhibits conductance values ~20% larger than those of the lower coordinated on top site.[36] The effect of increased coordination of the S atom may be more pronounced at step edges due to a stronger electronic coupling of S to Au and also, since the carbon atom adjacent to the S atom is close to the gold atoms of the upper gold layer (see Figure 9b). This proximity may facilitate direct electronic coupling of carbon to gold. However, to our knowledge, no conductance calculations for step-edge adsorption sites are available at present, and we hope to encourage theorists to work on this matter. Adsorption of the sulfur contacts at step edges may also stabilize the Au−S bond mechanically, which would probably increase the conductance as compared to the case of adsorption on atomically flat areas, where the adsorbed molecule is known to diffuse rapidly over the surface and formation and breaking of the Au−S bond is observed. However, to explore this effect theoretically will be rather demanding.

Summary

We have employed four different experimental methods ($I(s)$, $I(t)$, BJ, and MI) to determine the electrical conductance of alkanedithiols between gold contacts. Three different fundamental conductance groups have been observed for each molecule. The fundamental conductance values determined with the different methods were consistent, but the relative population of the different fundamental conductance groups depends on the type of method used to determine σ_M. A detailed gap separation analysis for each of the groups, together with measurements performed on surface areas with different step densities, provides evidence that the observation of the three fundamental σ_M groups can be attributed to different combinations of terrace and step-edge adsorption sites of the sulfur contacts, where adsorption on step edges increases the molecular conduction considerably. These findings are corroborated by a comparison of MI experiments, in which two different preparation techniques have been employed. The increased conductance observed at step edges may be explained by stronger electronic coupling of the molecule to the gold surface, by mechanical stabilization of the contact, or both; however, the role of atomic scale morphology in σ_M, as elucidated here, helps to explain the occurrence of three different conductance groups in single molecule conductance and holds significance for a better understanding of electron transfer through SAM systems.

Acknowledgment. This work was supported by EPSRC under Grants EP/C00678X/1, EP/DO7665X/1, and EP/D035678/1. S.M. acknowledges a postdoctoral fellowship from Ministerio de Educacion y Ciencia of Spain.

Supporting Information Available: Synthesis of dodecane-1,12-dithiol, single molecule conductance measurements using the $I(t)$ method, control experiments in the absence of molecules, voltage dependence of single molecule conductance, and comment on the $I(s)$ data analysis. This information is available free of charge via the Internet at http://pubs.acs.org/.

References and Notes

(1) Gray, H. B.; Winkler, J. R. *Proc. Nat. Acad. Sci.* **2005**, *102*, 3534–3539.

(2) Newton, M. D.; Smalley, J. F. *Phys. Chem. Chem. Phys.* **2007**, *9*, 555–572.

(3) Wang, W. Y.; Lee, T.; Reed, M. A. *Rep. Prog. Phys.* **2005**, *68*, 523–544.

(4) Reed, M. A.; Zhou, C.; Muller, C. J.; Burgin, T. P.; Tour, J. M. *Science* **1997**, *278*, 252–254.

(5) Weber, H. B.; Reichert, J.; Weigend, F.; Ochs, R.; Beckmann, D.; Mayor, M.; Ahlrichs, R.; von Lohneysen, H. *Chem. Phys.* **2002**, *281*, 113–125.

(6) Lortscher, E.; Weber, H. B.; Riel, H. *Phys. Rev. Lett.* **2007**, 98.

(7) Engelkes, V. B.; Beebe, J. M.; Frisbie, C. D. *J. Am. Chem. Soc.* **2004**, *126*, 14287–14296.

(8) Cui, X. D.; Zarate, X.; Tomfohr, J.; Sankey, O. F.; Primak, A.; Moore, A. L.; Moore, T. A.; Gust, D.; Harris, G.; Lindsay, S. M. *Nanotechnology* **2002**, *13*, 5–14.

(9) Cui, X. D.; Primak, A.; Zarate, X.; Tomfohr, J.; Sankey, O. F.; Moore, A. L.; Moore, T. A.; Gust, D.; Harris, G.; Lindsay, S. M. *Science* **2001**, *294*, 571–574.

(10) Morita, T.; Lindsay, S. *J. Am. Chem. Soc.* **2007**, *129*, 7262–7263.

(11) Xu, B. Q.; Tao, N. J. J. *Science* **2003**, *301*, 1221–1223.

(12) Haiss, W.; van Zalinge, H.; Higgins, S. J.; Bethell, D.; Hobenreich, H.; Schiffrin, D. J.; Nichols, R. J. *J. Am. Chem. Soc.* **2003**, *125*, 15294–15295.

(13) Haiss, W.; Nichols, R. J.; Higgins, S. J.; Bethell, D.; Hobenreich, H.; Schiffrin, D. J. *Faraday Discuss.* **2004**, *125*, 179–194.

(14) Haiss, W.; Nichols, R. J.; van Zalinge, H.; Higgins, S. J.; Bethell, D.; Schiffrin, D. J. *Phys. Chem. Chem. Phys.* **2004**, *6*, 4330–4337.

(15) Li, X. L.; He, J.; Hihath, J.; Xu, B. Q.; Lindsay, S. M.; Tao, N. J. *J. Am. Chem. Soc.* **2006**, *128*, 2135–2141.

(16) Li, C.; Pobelov, I.; Wandlowski, T.; Bagrets, A.; Arnold, A.; Evers, F. *J. Am. Chem. Soc.* **2008**, *130*, 318–326.

(17) Omori, Y.; Tobita, J.; Kato, Y.; Akiba, U.; Fujihira, M. *Jpn. J. Appl. Phys.* **2007**, *46*, 7829–7837.

(18) Nishikawa, A.; Tobita, J.; Kato, Y.; Fujii, S.; Suzuki, M.; Fujihira, M. *Nanotechnology* **2007**, *18*, 424005–424015.

(19) Weibel, N.; Blaszczyk, A.; von Haenisch, C.; Mayor, M.; Pobelov, I.; Wandlowski, T.; Chen, F.; Tao, N. J. *Eur. J. Org. Chem.* **2008**, 136–149.

(20) Venkataraman, L.; Klare, J. E.; Tam, I. W.; Nuckolls, C.; Hybertsen, M. S.; Steigerwald, M. L. *Nano Lett.* **2006**, *6*, 458–462.

(21) Jiang, J.; Kula, M.; Luo, Y. *J. Chem. Phys.* **2006**, 124.

(22) Sek, S.; Misicka, A.; Swiatek, K.; Maicka, E. *J. Phys. Chem. B* **2006**, *110*, 19671–19677.

(23) Wierzbinski, E.; Slowinski, K. *Langmuir* **2006**, *22*, 5205–5208.

(24) Suzuki, M.; Fujii, S.; Fujihira, M. *Jpn. J. Appl. Phys.* **2006**, *45*, 2041–2044.

(25) Li, X. L.; Hihath, J.; Chen, F.; Masuda, T.; Zang, L.; Tao, N. J. *J. Am. Chem. Soc.* **2007**, *129*, 11535–11542.

(26) He, J.; Chen, F.; Li, J.; Sankey, O. F.; Terazono, Y.; Herrero, C.; Gust, D.; Moore, T. A.; Moore, A. L.; Lindsay, S. M. *J. Am. Chem. Soc.* **2005**, *127*, 1384–1385.

(27) Jang, S. Y.; Reddy, P.; Majumdar, A.; Segalman, R. A. *Nano Lett.* **2006**, *6*, 2362–2367.

(28) Ren, B.; Picardi, G.; Pettinger, B. *Rev. Sci. Instrum.* **2004**, *75*, 837–841.

(29) Bethell, D.; Burst, M.; Schriffin, D. J.; Kiely, C. *J. Electroanal. Chem.* **1996**, *409*, 137–143.

(30) Beebe, J. M.; Kim, B.; Frisbie, C. D.; Kushmerick, J. G. *ACS Nano* **2008**, *2*, 827–832.

(31) Tomfohr, J. K.; Sankey, O. F. *Phys. Rev. B* **2002**, 65.

(32) Akkerman, H. B.; Blom, P. W. M.; de Leeuw, D. M.; de Boer, B. *Nature* **2006**, *441*, 69–72.

(33) Haiss, W.; Wang, C.; Grace, I.; Batsanov, A. S.; Schiffrin, D. J.; Higgins, S. J.; Bryce, M. R.; Lambert, C. J.; Nichols, R. J. *Nature Mat.* **2006**, *5*, 995–1002.

(34) Seminario, J. M.; Yan, L. M. *Int. J. Quantum Chem.* **2005**, *102*, 711–723.

(35) Jiang, J.; Lu, W.; Luo, Y. *Chem. Phys. Lett.* **2004**, *400*, 336–340.

(36) Lee, M. H.; Speyer, G.; Sankey, O. F. *Phys. Status Solidi B* **2006**, *243*, 2021–2029.

JP811142D